Spectral random masking: a novel dynamic masking technique for PIV in multiphase flows

Anders, S.; Noto, D.; Seilmayer, M.; Eckert, S.;

Originally published:

April 2019

Experiments in Fluids 60(2019)4, 68

DOI: https://doi.org/10.1007/s00348-019-2703-8

Perma-Link to Publication Repository of HZDR:

https://www.hzdr.de/publications/Publ-28683

Experiments in Fluids manuscript No.
(will be inserted by the editor)

Spectral Random Masking: A Novel Dynamic Masking Technique for PIV in Multiphase Flows

S. Anders · D. Noto · M. Seilmayer · S. Eckert

Received: date / Accepted: date

Abstract A novel masking technique for PIV-analysis of multiphase flows is presented. With this new approach, the velocity-field of an unmasked particle fraction (e. g. PIV-tracers) can be determined without the influence of a second (masked) particle fraction (e. g. bubbles or solid particles). Starting from a series of segmented grayscale images in which different particle fractions are determined for each frame, different masking techniques are compared. The problems caused by state of the art masking in case of dynamic masks (individual masks for each frame) are discussed. As a solution the novel spectral random masking algorithm is presented which replaces masked regions in the images by randomized intensity patterns in order to hide them from subsequent PIV-analysis. The advantages over conventional masking techniques are demonstrated for a model experiment of crystallizing ammonium-chloride solution.

Keywords PIV · Multiphase Flow · Image Masking

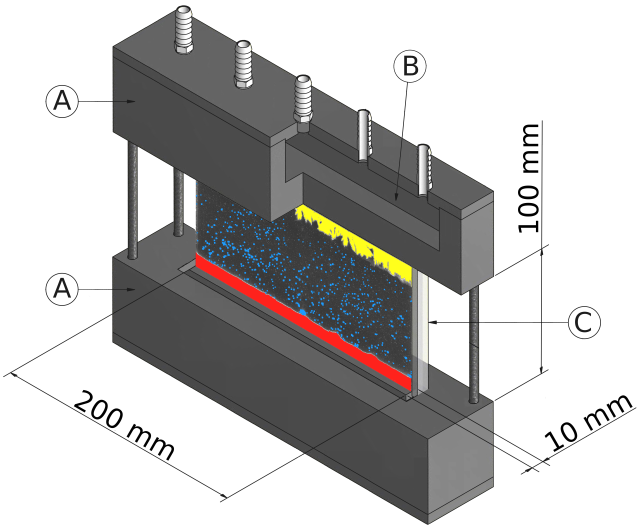

Fig. 1 Sketch of the experimental setup showing the copper blocks (A) with internal water baths (B). In place of the fluid container (C), a color coded snapshot of the experiment is inserted showing columnar crystals (yellow), sedimented crystals (red) and freely moving equiaxed crystals (blue)

1 Introduction

Particle Image Velocimetry (PIV) is a powerful technique for optical flow measurement which is commonly applied to single phase flows since decades. The application to multiphase flows however, can cause severe difficulties: Often erroneous displacement vectors are induced by moving objects of a second phase.

The present development is motivated by an experiment studying the interplay of solidification and double-diffusive convection (Anders and Eckert 2017). For this, a measurement cell (Fig. 1) was developed, which consists of a transparent fluid container clamped between two copper blocks controlling temperature at the upper and lower fluid boundary. The cell is filled with aqueous ammonium-chloride (NH_4Cl) solution. When this is supercooled, NH_4Cl solidifies as columnar crystals at the upper fluid boundary and as equiaxed crystals in the bulk liquid. The solidification regime and sedimentation of equiaxed crystals are both substantially influenced

S. Anders · M. Seilmayer · S. Eckert
Helmholtz-Zentrum Dresden-Rossendorf, Bautzner Landstraße 400, 01328 Dresden, Germany, Tel.: +49-351-2602901
E-mail: s.anders@hzdr.de

D. Noto
Lab. for Flow Control, Hokkaido University, N13 W8, Sapporo 060-8628, Japan, Tel.: +81-11-706-6373 E-mail: noto@ring-me.eng.hokudai.ac.jp

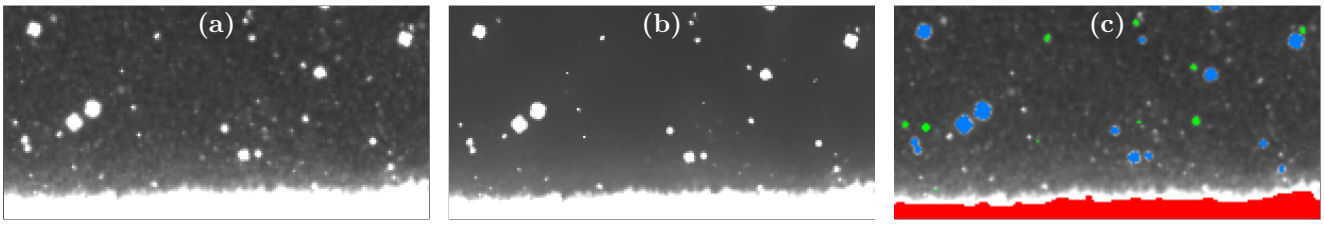

Fig. 2 Image segmentation process: **(a)** original grayscale image, **(b)** bilateral Gaussian blur applied to grayscale image, **(c)** color-coded segmented image showing sedimented crystals (red), equiaxed crystals (blue) and agglomerated tracers (green). The figures show detail views of 200 ×100 px

by double diffusive convection. A white LED light-sheet illuminates a plane in the center of the fluid container of 4 to 5 mm thickness. This thickness is necessary to reduce shadows caused by the dispersed phase and to enable the reliable detection and quantification of the latter. Image sequences are recorded with a single camera at which the choice of lens and aperture ensures a depth of field large enough to reproduce sharp phase boundaries over the full depth of the fluid container. The main objective of the experiment is to simultaneously measure the flow in the fluid and to determine the growth and the trajectories of the salt crystals.

Measuring individual velocity fields of the continuous and the dispersed phase in multiphase flows is a challenging task for PIV. If the two phases cannot be separated during image acquisition and have only a small density contrast, they can only be distinguished by extensive image preprocessing and the dispersed phase needs to be masked during PIV-analysis of the continuous phase (compare Khalitov and Longmire 2002). In many experiments however, the illumination in combination with the dispersed phase causes reflections, shadows and other image distortions (Brücker 2000). This leads to an image background which is neither black nor homogeneous and has only a small contrast to the PIV-tracers. As will be shown later, in this case state of the art masking techniques are not capable of dynamically masking a second phase in the sense that...

- no erroneous correlation peaks are introduced to the PIV-analysis;
- no velocity information is lost near phase boundaries.

To overcome these difficulties, a novel method for effective dynamic masking of PIV-images was developed and will be presented in the following.

2 Image processing

To illustrate and compare the spectral random masking scheme, a representative time interval of an experiment was chosen. During this, a moderate convective flow together with growth and sedimentation of columnar and equiaxed crystals is present.

The image acquisition yields 2 Mpx intensity images $\mathbf{I}_{\mathrm{org}}$ with a resolution of 10 px/mm and 8 bit coded pixels $p_{i,j}$ (see Fig. 2(a)). To identify the different objects, these images are going to be segmented into different classes x with corresponding binary masks $\mathbf{M}_{\mathrm{x}}$. A region R_k of some mask $\mathbf{M}$ is defined as the set of coordinate pairs $\{(i,j)_1,\ldots,(i,j)_n\}_k$ with the following properties: (i) All pixels of R_k are marked as "True" by the corresponding mask; (ii) ... All pixels of R_k share at least one edge with another pixel of the same R_k. The regions size is defined as its cardinal number $|R_k|$.

Image segmentation First, a minimum image is computed by taking the minimum intensity value of each pixel during a period without crystallization. This is then thresholded to generate a static mask $\mathbf{M}_{\mathrm{stat}}$ which filters visual artifacts stemming from the fluid container's walls. A bilateral Gaussian blur is applied to each $\mathbf{I}_{\mathrm{org}}$ to reduce high frequency noise while preserving sharp phase boundaries (see Fig. 2(b)). Next, large regions of columnar and sedimented crystals $\mathbf{M}_{\mathrm{col}}$ (red region in Fig. 2(c)) are detected by global thresholding. In contrast to this, smaller particles are detected by locally-adaptive thresholding. For this, two classes are defined: Larger and brighter particles are classified as equiaxed crystals $\mathbf{M}_{\mathrm{equ}}$ (blue regions in Fig. 2(c)) and smaller, less bright particles as agglomerated tracers $\mathbf{M}_{\mathrm{trc}}$ (green regions in Fig. 2(c)). $\mathbf{M}_{\mathrm{trc}}$ suppresses spurious displacement vectors in the subsequent PIV-analysis while allowing $\mathbf{M}_{\mathrm{equ}}$ to only contain crystals (see Khalitov and Longmire 2002 for details of segmentation methods). The segmentation process was implemented with a focus on avoiding false positive crystal detection.

Image masking The starting point for the masking process are the segmented images or the set of masks $\mathbf{M}_{\mathrm{x}}$ respectively. Due to the rather exclusive threshold values used during image segmentation, some of the regions $R_{\mathrm{x}k}$ exhibit a bright aura (see Fig. 2(c)) that would disturb the PIV-evaluation. Therefore, the $R_{\mathrm{x}k}$ are dilated

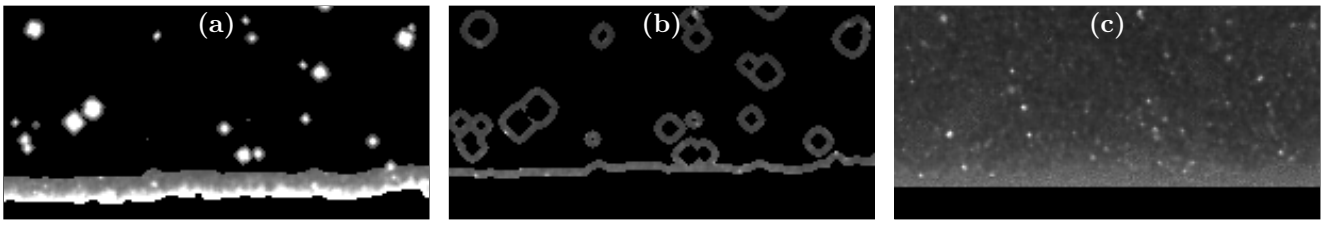

Fig. 3 Spectral random masking process: **(a)** pixel regions to randomize, **(b)** pixel regions to use as local intensity samples, **(c)** randomized grayscale image as used for PIV-analysis. The figures show detail views of 200 ×100 px

to a variable extent depending on their class x and their individual size. The corresponding kernels range from a cross shape of 3 ×3 px for $R_{\mathrm{stat}\,k}$ with a size of 3 to 6 px to a box shape of 13 ×13 px for $R_{\mathrm{col}\,k}$. The kernels were determined individually for the different masks by trial and error to capture only the bright auras around the masked regions. Next, the dilated masks are joined and remaining holes of a few pixels size are removed. These morphological manipulations result in $\mathbf{M}_{2\mathrm{msk}}$ masking all pixels that should not be regarded for the velocity computations.

After that, common techniques offer two main options: The first is to pad all $R_{2\mathrm{msk}\,k}$ with either a constant intensity value, i. e. zero padding, or with random intensity values of some constant range, i. e. random padding, and subsequently computing the displacement field from the resulting images $\mathbf{I}_{\mathrm{piv}}$. This only yields satisfying results in case of a homogeneous background with enough contrast to the tracer particles and relatively small regions $R_{2\mathrm{msk}\,k}$. The second option, i. e. vector masking, is to compute the displacement field for the unmasked images $\mathbf{I}_{\mathrm{org}}$ and subsequently mask the resulting vectors with $\mathbf{M}_{2\mathrm{msk}}$. This only yields satisfying results if the regions $R_{2\mathrm{msk}\,k}$ are further apart than the size of the PIV-interrogation windows. In consequence, the displacement field cannot be determined close to phase boundaries (Seol and Socolofsky 2008).

These limitations can be overcome by the spectral random masking scheme which fills the regions $R_{2\mathrm{msk}\,k}$ with noise possessing a similar intensity spectrum as the local background. This is achieved by randomly sampling the neighborhood of each $R_{2\mathrm{msk}\,k}$.

Since the mask for sedimented and columnar crystals covers regions much bigger than the PIV-interrogation windows, computational effort can be reduced by excluding $\mathbf{M}_{\mathrm{col}}$ from randomization. This yields the mask $\mathbf{M}_{2\mathrm{rnd}}$, defining all regions to be randomized $R_{2\mathrm{rnd}\,l}$ (Fig. 3(a)). The mask for the sample regions, is the result of the logic operation $\mathbf{M}_{4\mathrm{smp}} = \mathbf{M}_{\mathrm{dil}} \wedge \neg(\mathbf{M}_{2\mathrm{msk}} \vee \mathbf{M}_{\mathrm{col}})$. Here $\mathbf{M}_{\mathrm{dil}}$ is the dilation of $\mathbf{M}_{2\mathrm{rnd}}$ with a disc shaped kernel of 9 ×9 px. The kernel's size was determined as a compromise between sample areas large enough to capture the intensity spectrum and acceptable computing time. In addition, care was taken not to generate large overlapping sample areas for numerous $R_{2\mathrm{rnd}\,k}$ as this would compromise the localized sampling of the intensity spectrum. The resulting $\mathbf{M}_{4\mathrm{smp}}$ displays ring-like structures around every smaller region to randomize and an elongated region next to the large regions of $\mathbf{M}_{\mathrm{col}}$ (compare Fig. 3(a) and (b)). This fulfills the condition $\mathbf{M}_{4\mathrm{smp}}[\mathbf{M}_{2\mathrm{rnd}} == 1] == 0$.

Through matching of the Cartesian bounding box of each sample region $R_{4\mathrm{smp}_k}$ with the center of the corresponding $R_{2\mathrm{rnd}\,l}$, pairs (k, l) are determined. To limit the effect of single bright tracers during sampling, the spectrum of each $R_{4\mathrm{smp}_k}$ is individually cutoff at $I_{\mathrm{max}\,k} = 2 \cdot I_{\mathrm{med}\,k} - I_{\mathrm{min}\,k}$ where $I_{\mathrm{med}\,k}$ is the median and $I_{\mathrm{min}\,k}$ the minimum intensity of $R_{4\mathrm{smp}_k}$. This specific cutoff ensures, that the sampled intensity range adapts automatically to the varying illumination and seeding conditions encountered during the different experimental runs. Any trial and error to find a suitable value for a constant I_{max} is avoided. Due to shadows caused by the dispersed phase, individual sample regions often display spatial intensity gradients. This is respected by a bilinear fit $f_k(i, j)$ of the spatial intensity distribution inside every single $R_{4\mathrm{smp}_k}$. The new intensity values I_{msk} for each pixel $p_{i,j}$ of each region $R_{2\mathrm{rnd}\,l}$ are computed by randomly choosing values from the corresponding $R_{4\mathrm{smp}_k}$ and shifting these values according to the fit function f_k of $R_{4\mathrm{smp}_k}$ and the coordinates (i, j).

This randomization scheme assures three things: Masked regions...

- exhibit the intensity spectrum of their neighborhood;
- of consecutive frames do not correlate;
- possess a smooth transition to the background even in cases of strong local intensity gradients.

Fig. 3(c) illustrates the result of spectral random masking: The dispersed phase becomes almost indistinguishable from the background and only the interior of large masked regions is masked by zero padding. The image processing procedure described above is illustrated in a flow chart (Online Resource 1).

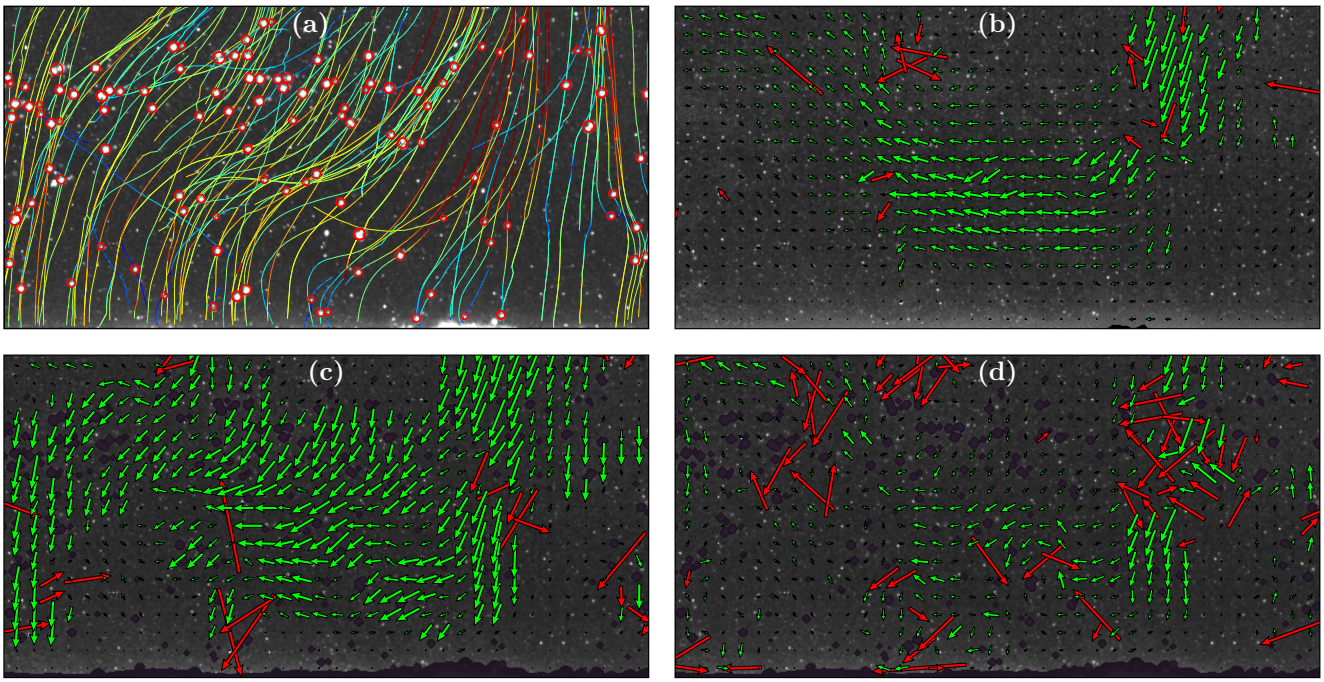

Fig. 4 Comparison of results for different masking methods: **(a)** trajectories of salt crystals where the line-color corresponds to instantaneous velocity and red circles denote the current particle positions. PIV-result of continuous phase for **(b)** spectral random masking, **(c)** zero padding, **(d)** random padding. In **(c)** and **(d)** the movement of salt crystals crosstalks into the PIV-correlation resulting in incorrect velocity fields. In **(b)-(d)** red arrows denote erroneous and green arrows valid displacement vectors. The figures show detail views of 616 ×308 px at the bottom center of the fluid container

3 PIV-analysis

The PIV-evaluation was conducted with the software *PIVview* version 3.6.0 together with the parameters listed in Tab. 1. These parameters were applied to three different masking schemes (zero and random padding as well as spectral random masking) without modification. Fig. 4(b) to (d) show the results of the outlier detection filter which is applied after the correlation steps. The detail chosen for these figures represents a region near the bottom center of the fluid container. Here, the velocity field of the continuous phase shows a wave-like pattern starting with a downward flow slightly inclined to the left just right of the image center. This evolves into a left-inclined upward flow in the left part of the image.

To compare the effectiveness of the different masking schemes, the displacement of the salt crystals also needs to be taken into account. The crystal positions as determined through image segmentation (see Fig. 2(c)) are linked with a nearest neighbor particle tracking algorithm similar to (Kelley and Ouellette 2011). The resulting trajectories are shown in Fig. 4(a). In the center of the detail view, the crystals basically move in parallel to the velocity field of the continuous phase. In the left part however, the trajectories indicate a sedimentation of the crystals against the upward flow of the continuous phase.

The result of spectral random masking (Fig. 4(b)) shows a smooth velocity field of the continuous phase throughout the whole detail view. Especially in the left third of the image it is obvious, that the sedimenting crystals have no substantial influence on this PIV-evaluation. Comparing the number of physically correct displacement vectors (which are not necessarily equivalent to vectors qualified as “valid” by the statistical outlier detection), it becomes clear, that spectral random masking outperforms traditional masking techniques: The result for zero padding (Fig. 4(c)) in-

Table 1 Parameter used during PIV-analysis

parameter	value	description
grid	48 × 48	64% overlap
correlation	FFT	3 rpt. correl.
interrogation	multipass	4 passes
image interpol.	B-Spline	3rd order
sub-px peak fit	LSQ Gauss	3 × 3 points
norm. med. thresh	15.0 px	
max disp. test	20.0 px	
max disp. diff.	8.0 px	outlier detection
z-score	5.0	
dyn. mean test	$1 \cdot \bar{d} \pm 3 \cdot \mathrm{Var}(d)$	

dicates a uniform downward flow for the left fringe of the detail view. This is more representative for the sedimentation of the dispersed phase. In such a case of a locally smooth velocity field, statistical outlier detection generates false positive vectors. The result for random padding (Fig. 4(d)) is even more inconsistent: Some of the displacement vectors seem to characterize the sedimentation movement while others characterize the flow of the continuous phase. In addition random padding causes many arbitrary displacement vectors as indicated by the outlier detection.

A full quantification of the benefits of spectral random masking would require a detailed bench-marking against synthetic test images and will be subject to future publication. However, the authors believe, that the given qualitative analysis already shows, that the novel masking scheme yields physically reasonable results in cases where state of the art masking methods do not allow to compute any velocity field representing the correct phase. Even if one would accept a larger number of erroneous vectors, a statistical outlier detection does not lead to reasonable and robust results as illustrated above.

4 Summary and outlook

A novel method for dynamic masking during multi-phase PIV has been developed and successfully applied to a model experiment of a solidifying NH_4Cl solution. In contrast to other methods, spectral random masking effectively hides the dispersed phase from PIV-analysis of the continuous phase in a way, that almost no erroneous vectors are induced to the resulting velocity field. This enables quantitative studies even in case of a finely scattered dispersed phase and it allows for velocity measurements in the direct vicinity of phase boundaries. Unlike other multiphase masking techniques (e. g. Gui et al. 2003), the method described here does not require any adaption of the PIV-correlation method and therefore is universally applicable. A video showing the application of spectral random masking to an image sequence from the experiment described in section 1 can be found in Online Resource 2.

While this publication already showed the capabilities of the new method, some options for further refinements exist: Sampling could be implemented as an even more adaptive process sensitive to size, intensity distribution or shape of the individual regions to mask. In addition, a randomization scheme reproducing texture features of the local background could extend the possible applications beyond the masking of PIV-images. To determine the effectiveness of these possibilities together with optimal parameters, a detailed bench-marking using artificial image sets will be necessary. For the experiment described in this paper however, these aspects were not considered as relevant in order to determine independent velocity fields for the different particle fractions. In addition, the projected experimental studies require to analyze hundreds of thousands of images and thus computing time becomes an additional limiting resource for further refinements.

Acknowledgements The authors acknowledge financial support by the German Research Foundation (DFG) in the framework of the SPP 1488 “Planetmag”, Grant EC 217/1-1.

References

Anders S, Eckert S (2017) Interaction between double diffusive convection and solidification in ammonium-chloride solutions. In: Fan Z (ed) Proceedings of the 6th Decennial International Conference on Solidification Processing, BCAST, Brunel University London, Old Windsor, UK, pp 350–353

Brücker C (2000) PIV in two-phase flows. In: Riethmuller M (ed) Particle Image Velocimetry and Associated Techniques, Lecture Series 2000-01, Von Karman Institute for Fluid Dynamics, Rhode-St. Genese, Belgium

Gui L, Wereley ST, Kim YH (2003) Advances and applications of the digital mask technique in particle image velocimetry experiments. Meas Sci Technol. https://doi.org/10.1088/0957-0233/14/10/312

Kelley DH, Ouellette NT (2011) Using particle tracking to measure flow instabilities in an undergraduate laboratory experiment. Am J Phys. https://doi.org/10.1119/1.3536647

Khalitov DA, Longmire EK (2002) Simultaneous two-phase PIV by two-parameter phase discrimination. Exp Fluids. https://doi.org/10.1007/s003480100356

Seol DG, Socolofsky SA (2008) Vector post-processing algorithm for phase discrimination of two-phase PIV. Exp Fluids. https://doi.org/10.1007/s00348-008-0473-9